Article

Neuron

Context-Dependent Sensory Processing across Primary and Secondary Somatosensory Cortex

Graphical Abstract

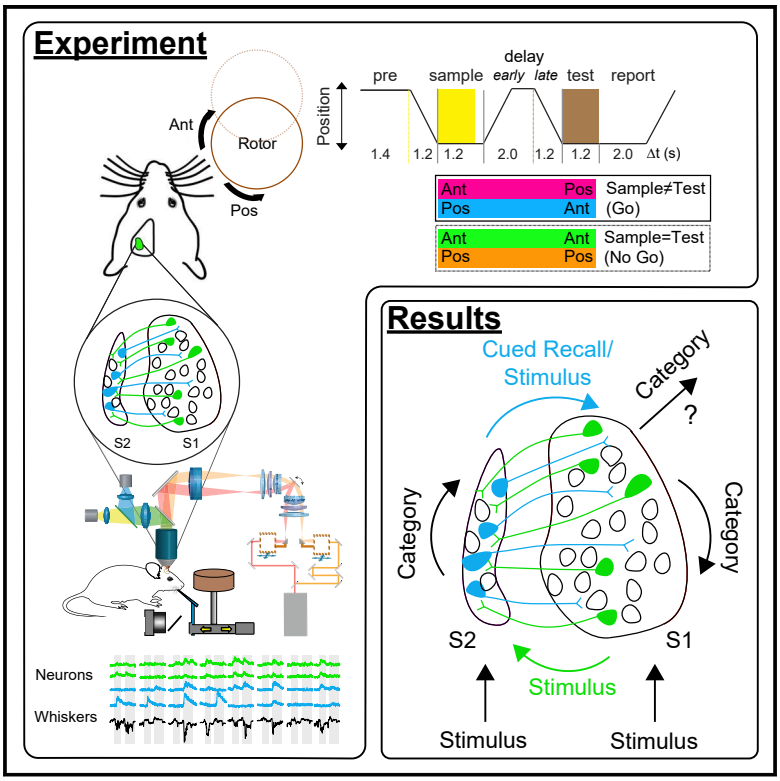

Highlights

- Mouse S1 and S2 encode overlapping information during a tactile working memory task
- Recall responses of previous stimuli are more prevalent in S2 and are relayed to S1
- Category information in S1, but not S2, is necessary for task performance
- Network properties of S2 allow task information to persist across behavior states

Authors

Cameron Condylis, Eric Lowet, Jianguang Ni, Karina Bistrong, Timothy Ouellette, Nathaniel Josephs, Jerry L. Chen

Correspondence

jerry@chen-lab.org

In Brief

Condylis, Lowet, et al. investigate the roles of the primary and secondary somatosensory cortex during a tactile working memory task in mice. The authors find that during context-dependent sensory processing, handling of specific types of task-related information can occur in either a segregated or distributed manner across both areas.

Condylis et al., 2020, Neuron *106*, 1–11
May 6, 2020
https://doi.org/10.1016/j.neuron.2020.02.004

CellPress

Please cite this article in press as: Condylis et al., Context-Dependent Sensory Processing across Primary and Secondary Somatosensory Cortex, Neuron (2020), https://doi.org/10.1016/j.neuron.2020.02.004

Neuron
Article

Context-Dependent Sensory Processing across Primary and Secondary Somatosensory Cortex

Cameron Condylis,[1,6] Eric Lowet,[2,3,6] Jianguang Ni,[2,3] Karina Bistrong,[2] Timothy Ouellette,[2] Nathaniel Josephs,[4] and Jerry L. Chen[1,2,3,5,7,*]
[1]Department of Biomedical Engineering, Boston University, Boston, MA 02215, USA
[2]Department of Biology, Boston University, Boston, MA 02215, USA
[3]Center for Systems Neuroscience, Boston University, Boston, MA 02215, USA
[4]Department of Mathematics and Statistics, Boston University, Boston, MA 02215, USA
[5]Senior author
[6]These authors contributed equally
[7]Lead Contact
*Correspondence: jerry@chen-lab.org
https://doi.org/10.1016/j.neuron.2020.02.004

SUMMARY

To interpret the environment, our brain must evaluate external stimuli against internal representations from past experiences. How primary (S1) and secondary (S2) somatosensory cortices process stimuli depending on recent experiences is unclear. Using simultaneous multi-area population imaging of projection neurons and focal optogenetic inactivation, we studied mice performing a whisker-based working memory task. We find that activity reflecting a current stimulus, the recollection of a previous stimulus (cued recall), and the stimulus category are distributed across S1 and S2. Despite this overlapping representation, S2 is important for processing cued recall responses and transmitting these responses to S1. S2 network properties differ from S1, wherein S2 persistently encodes cued recall and the stimulus category under passive conditions. Although both areas encode the stimulus category, only information in S1 is important for task performance through pathways that do not necessarily include S2. These findings reveal both distributed and segregated roles for S1 and S2 in context-dependent sensory processing.

INTRODUCTION

How a sensory stimulus is interpreted depends on the context in which it is perceived. This context can include other incoming stimuli from the surrounding sensory scene or can be composed of internal representations of relevant past sensory experiences and behavioral states (Khan and Hofer, 2018). Context-dependent sensory processing can produce new categorical representations that can reflect the integration and comparison of past and present stimuli (Miller et al., 1991; Romo et al., 2012). How the neocortex is organized to produce such category representations is largely unclear. Sensory cortices are parcellated into primary and higher areas in which neurons in higher areas can encode for increasingly invariant representations (DiCarlo et al., 2012; Kitada, 2016). However, the extent to which context-dependent sensory processing occurs in a serial, hierarchical manner (Felleman and Van Essen, 1991) or in a distributed fashion (Rumelhart and McClelland, 1987; Siegel et al., 2015) across these cortical areas remains a topic of debate.

The recent availability of increasingly large-scale, cellular recording techniques now enables a thorough survey of the diversity of neuronal responses and the dynamic interactions that exist across cortical areas (Jun et al., 2017; Sofroniew et al., 2016). New evidence suggests that the encoding of task-related information can be highly distributed across related cortical areas, which supports the notion of a distributed network for perceptual processing (Chen et al., 2016; Hernández et al., 2010; Koay et al., 2019; Minderer et al., 2019; Steinmetz et al., 2018). However, functional recordings alone do not provide insight as to whether such widespread signals are due to local processing within an area or the inheritance of information from other connected areas. Therefore, population coding and information flow between areas must also be tracked. Further, functional perturbations in each area must be performed to determine whether information available locally within an area is necessary for sensory-driven behavior.

Here, we investigate how the primary (S1) and secondary (S2) whisker somatosensory cortex operate and interact to process tactile stimuli and their related context. Large-scale multi-area imaging across S1 and S2 confirms the presence of a distributed code in which both areas contain activity that reflects the present stimulus, the recall of recent stimulus representations, and stimulus context. However, through local optogenetic inactivation and activity measurements in anatomically identified cortico-cortical projection neurons, we find that the functional roles of these areas are not identical but instead reflect computations where the processing of recently recalled sensory stimuli can

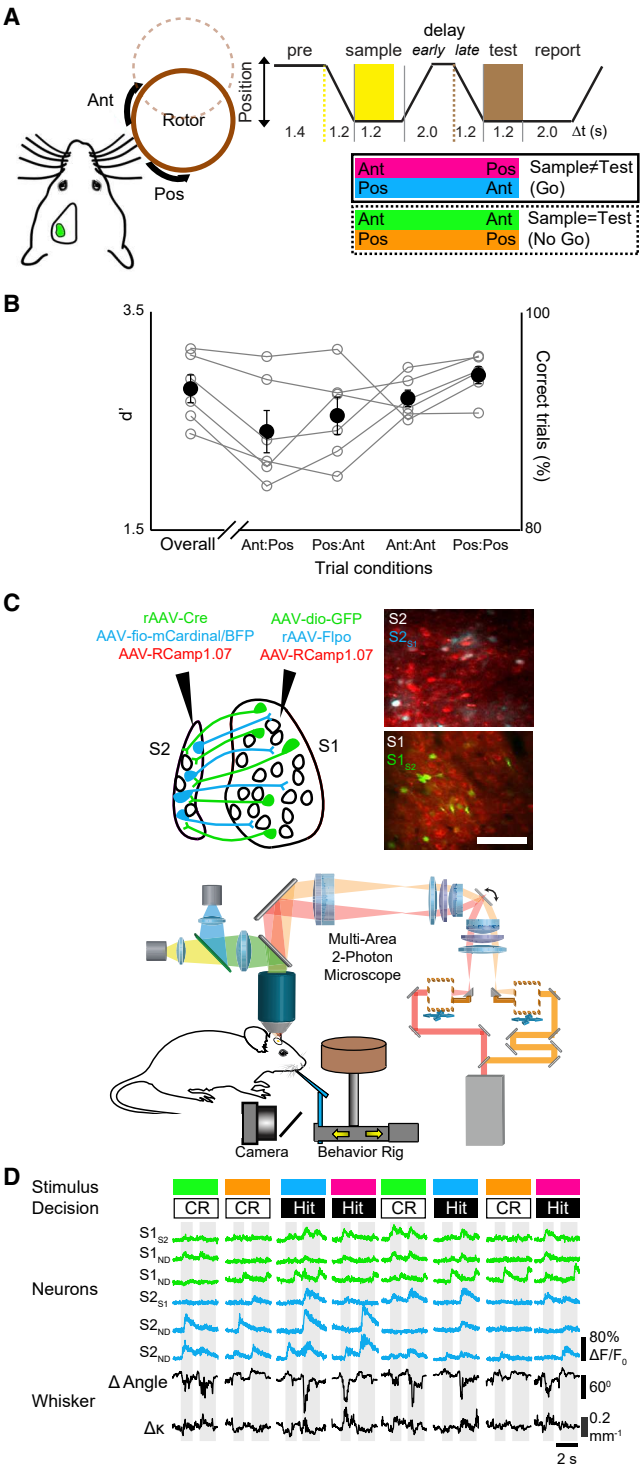

Figure 1. Multi-area Two-Photon Imaging across S1 and S2 during a Delayed Non-match-to-Sample Task

(A) Schematic of behavioral task.

(B) Behavior performance from two-photon imaging experiments. Overall performance across recording sessions is shown along with performance for each trial condition. Performance for individual animals (open circles) is shown along with the mean for all animals (black circle). Error bars indicate SEM.

(C) Schematic of multi-area imaging experiment including a viral injection scheme for calcium indicator expression and labeling of projection neurons (upper left) and example *in vivo* two-photon images of expression in S1 and S2 (upper right). Scale bar indicates 100 μm; head-fixed mouse under multi-area two-photon microscope and behavioral rig (bottom).

(D) Example simultaneous recordings from S1 and S2 neurons during behavioral task along with extracted periods of whisker-to-rotor touch (gray area), whisker angle, and whisker curvature from high speed videography.

be attributed to S2, whereas the processing of stimuli and their context is distributed in parallel across S1 and S2.

RESULTS

Simultaneous Multi-area Population Imaging during a Tactile Working Memory Task

In order to study context-dependent sensory processing in adult mice, we developed a head-fixed whisker-based delayed non-match to sample (DNMS) task that required the animal to compare past and present stimuli (Figure 1A). In the task, a rotating rotor was used to deflect whiskers in either an anterior or posterior direction. An initial 1.2-s "sample" stimulus was presented, followed by a 2-s delay, and then by a 1.2-s "test" stimulus. During the delay period and the inter-trial interval, the rotor was withdrawn to prevent whisker-rotor contact. Behavior was reported as "go/no-go," in which animals licked on "go" trials for a water reward ("hit") when the presented sample and test stimulus were non-matching and withheld licking on "no-go" trials ("correct rejection") when the presented sample and test stimulus were matching. Misses on go trials were not rewarded, and false alarms on no-go trials were punished with an air puff and a time-out period. Expert animals could reach high performance levels ($d' = 2.79 \pm 0.12$) (Figure 1B), performing ~300 trials per session.

In order to investigate neuronal dynamics within and across S1 and S2 during the DNMS task, we applied a recently developed multi-area two-photon microscope (Chen et al., 2016) to simultaneously measure population calcium activity across the two areas by using a red genetically encoded calcium indicator, RCaMP1.07 (Ohkura et al., 2012) (Figures 1C and 1D). We used viral-mediated retrograde tracers (Tervo et al., 2016) expressing Cre-dependent and Flpo-dependent fluorescent reporters to additionally identify $S1_{S2}$ ("feedforward") and $S2_{S1}$ ("feedback") neurons from unlabeled, not-determined neurons ($S1_{ND}$ and $S2_{ND}$), similar to as previously described (Chen et al., 2016). By doing so, $S1_{S2}$ neurons identified by GFP expression in S1 and $S2_{S1}$ neurons could be identified by mCardinal-NLS or mTagBFP2-H2B expression in S2. We imaged activity from 6,603 neurons (3,661 $S1_{ND}$ neurons, 156 $S1_{S2}$ neurons, 2,645 $S2_{ND}$ neurons, and 141 $S2_{S1}$ neurons) across 6 animals for 8 to 14 sessions per animal. In addition, we used high-speed videography to monitor whisker kinematics during rotor touch and rotation.

Task-Related Whisker Kinematics Features

To first characterize how task stimuli drive whisker kinematics, we analyzed periods of whisker-rotor touch and changes in the mean whisker angle and curvature during rotor rotation (Clack

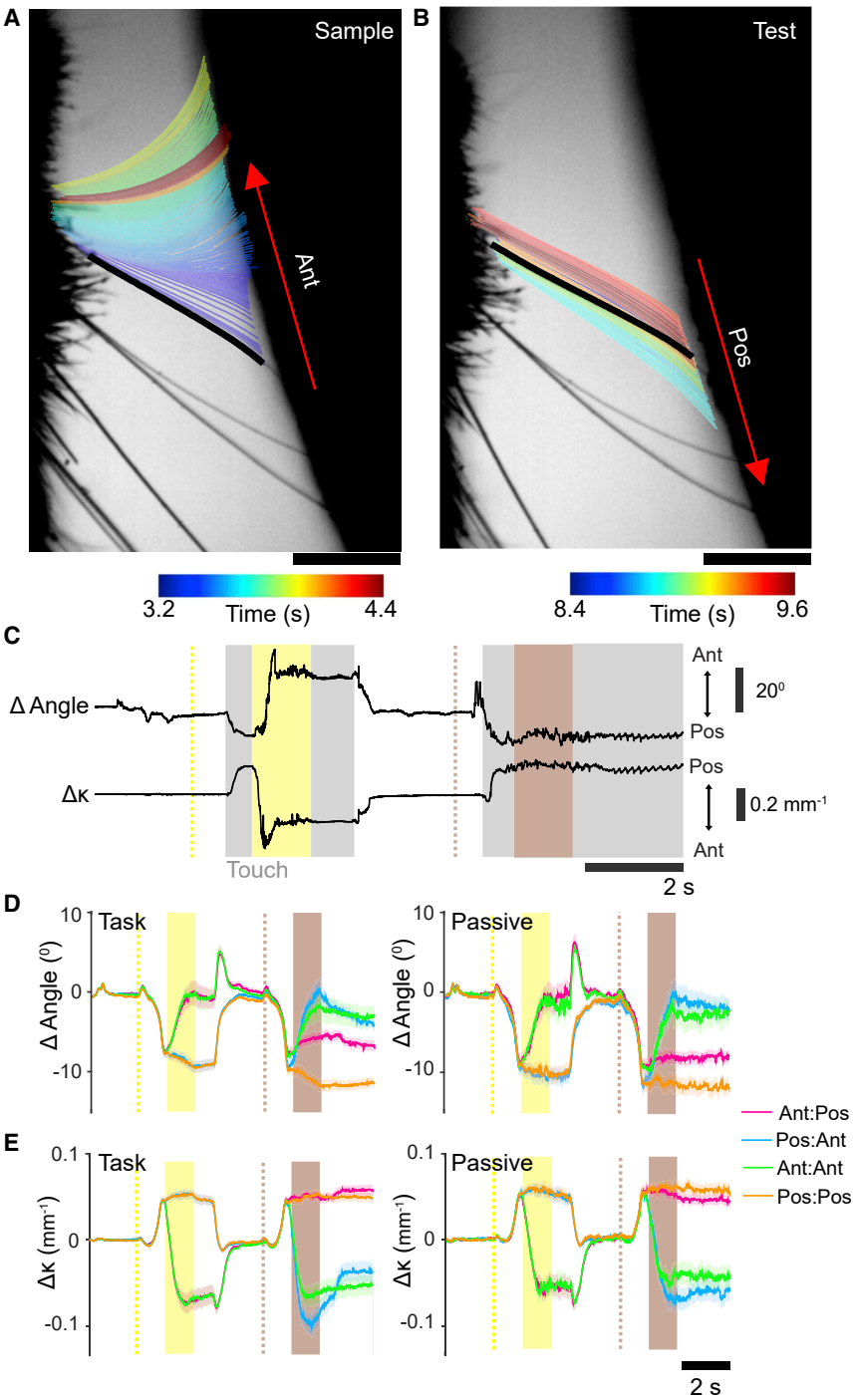

Figure 2. Whisker Kinematics across Task and Passive Conditions

(A) Example trace of an anterior whisker deflection during the sample period.

(B) Example trace of a posterior whisker deflection during the sample period.

(C) Calculated angle and curvature changes for the whisker tracked in (A) and (B) during a single trial.

(D) Trial-averaged angle changes across behavioral sessions for each trial condition during task (left) and passive (right) conditions.

(E) Trial-averaged curvature changes across behavioral sessions for each trial condition during task (left) and passive (right) conditions. Scale bar indicates 1 mm. Error bars indicate SEM; n = 53 imaging sessions.

See also Figure S1.

et al., 2012) (Figures 2A–2C). Initial whisker-rotor contact prior to the rotation of the sample or test stimulus produced whisker deflections and curvature changes in the posterior direction. During the sample and test period, anterior or posterior rotation produced angle and curvature changes ($\Delta\kappa$) in their respective directions (Figures 2D and 2E). Withdrawal of the rotor after anterior rotation occasionally produced additional anterior deflections and curvature changes as whiskers were pulled along with the retracting rotor (Figure S1). Once the rotor was beyond whisker contact, whisker kinematics returned to pre-stimulus conditions, suggesting that the identity of the sample stimulus was not maintained by whisker kinematic properties by the end of the delay period (angle: $p = 0.25$, $\Delta\kappa$: $p = 0.06$, paired t test). Whisker kinematics were comparable between task and passive stimulation conditions, suggesting that active whisking strategies observed in other tasks (Chen et al., 2015; O'Connor et al., 2010) were not a prominent behavioral feature of this particular task.

Heterogeneous Representation of Task-Related Information

Although whisker S1 and S2 have been observed to encode stimulus and choice-related activity (Chen et al., 2016; Kwon et al., 2016; Yamashita and Petersen, 2016; Yang et al., 2016), the extent to which more complex, context-modulated information is also present has been less investigated. To assess the diversity of task-related responses, during the trial, we fit deconvolved calcium signals to three regressors that would allow us to explain a neuron's firing rate as a combination of (1) the sample stimulus (β_{sample}), (2) the test stimulus (β_{test}), and (3) the trial category ($\beta_{category}$), as inferred by activity specific to the combination of sample and test stimuli ("non-match" versus "match") or the animal's choice ("hit" versus "correct rejection") (Figures 3A, 3B, and S2A–S2D). Direction-tuned neurons were prominently observed in both the areas as indicated by neurons coding for sample information during the sample period (β_{sample} [sample]) and test information during the test period (β_{test} [test]). Direction tuning was maintained in individual neurons between the sample

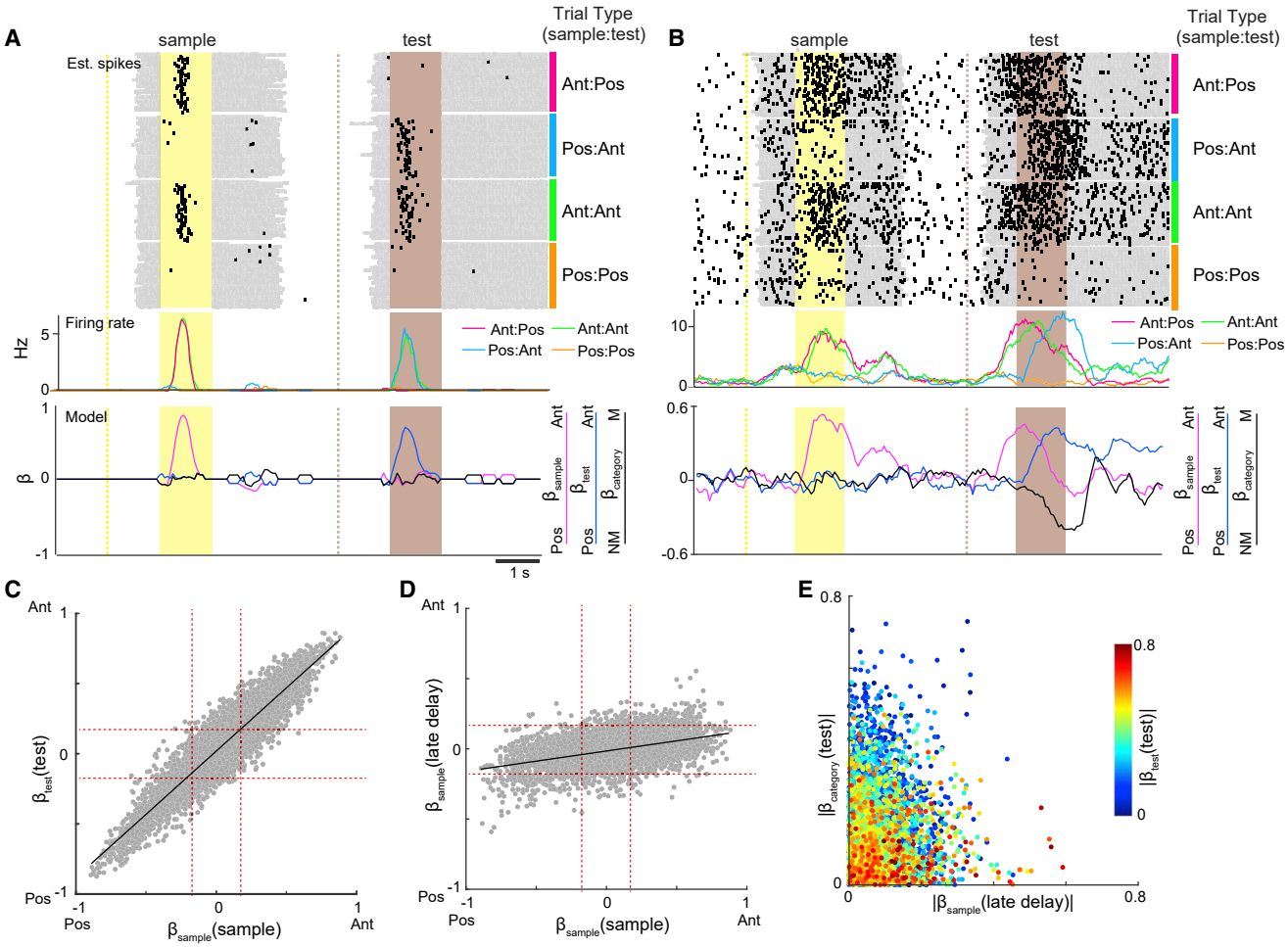

Figure 3. Decoding Task Variables in Single Neurons by Multiple Regression Analysis

(A) An example stimulus-selective neuron. Top shows estimated spikes across trials sorted by stimulus conditions. Middle shows mean firing rate for each stimulus condition. Bottom shows decoded task variables across the trial period.

(B) An example neuron with context-dependent responses. The top shows estimated spikes across trials sorted by stimulus conditions. Middle shows mean firing rate for each stimulus condition. The bottom shows decoded task variables across the trial period.

(C) Scatterplot of β_{sample} (sample) versus β_{test} (test), demonstrating that neurons maintain stimulus preference in both the sample and test period. Dotted red line corresponds to significance level from shuffling.

(D) Scatterplot of β_{sample} (sample) versus β_{sample} (late delay), demonstrating that sample stimulus information is present in the late delay period. Dotted red line corresponds to significance level from shuffling.

(E) Scatterplot of β_{sample} (late delay) versus β_{test} (test) versus β_{test} (category), demonstrating that sample, test, and category information are heterogeneously distributed across individual neurons. n = 6,603 neurons.

See also Figures S2 and S4.

and test period (Figure 3C) ($R = 0.92$, $p < 1 \times 10^{-300}$). Although activity tuned to the sample stimulus was not maintained throughout the delay period (Figures S2E, S2F, and S6), sample-tuned activity re-emerged in some neurons late in the delay period (β_{sample} [late delay]) that extended into the test period (Figure 3D) ($R = 0.43$, $p < 1 \times 10^{-292}$). In addition to the sample and test stimulus information, information related to the trial category was also present during the test period ($\beta_{category}$ [test]). Analysis of the distribution of sample, test, and category responses shows that individual neurons vary widely in both the degree and type of information they encode (Figures 3E and S2D). These results demonstrate that S1 and S2 can encode complex sensory responses that include information about the preceding stimulus and context-dependent modulation of incoming stimuli resulting in categorical responses.

Cued-Recall Response during the Late Delay Period

The re-emergence of sample information late in the delay period was surprising given that persistent delay activity was not observed in S1 and S2. We hypothesized that such information could represent a "cued recall" in which whisker touch by the re-approaching rotor prior to test stimulus delivery served as a cue. We generated peri-touch time histograms for neuronal firing rate and sample information (Figures 4A and 4B). Cued recall neurons were defined as exhibiting significant $|\beta_{sample}|$ during

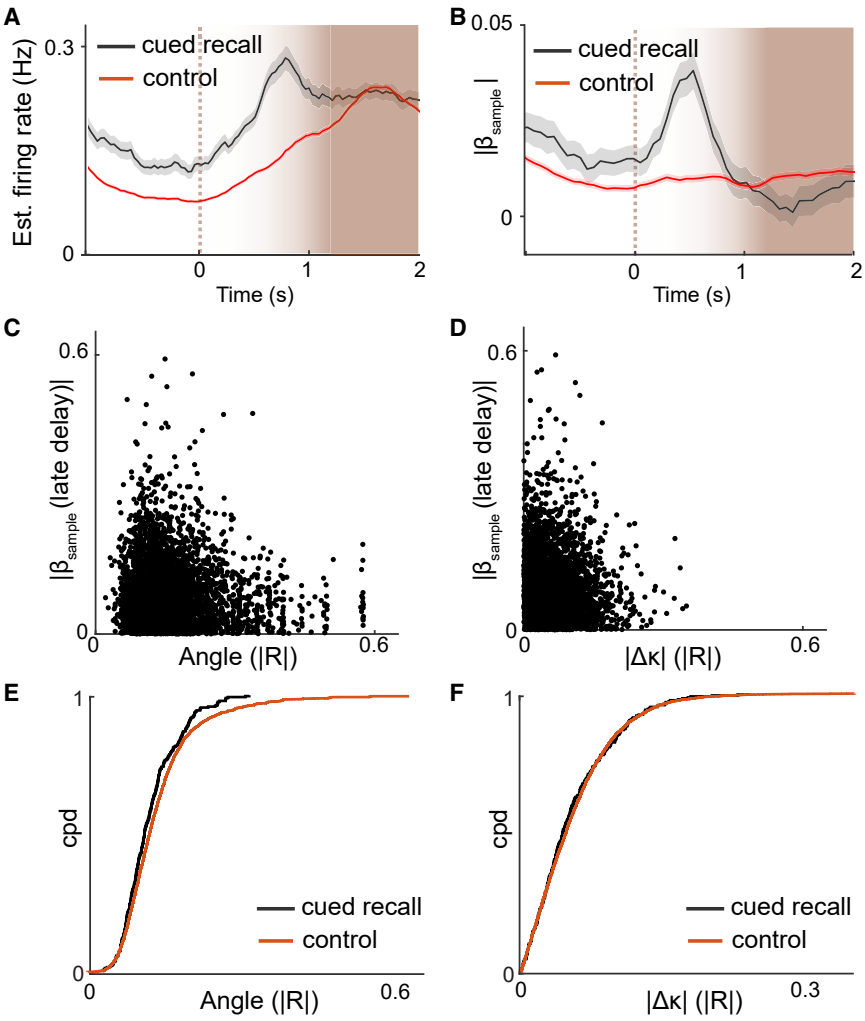

Figure 4. Sample Recall Emerges upon Whisker Touch Late in the Delay Period

(A) Average firing rate during the late delay period aligned to whisker-rotor touch onset for neurons with cued recall responses, i.e., significant $|\beta_{sample}$ (late delay)| versus control neurons.

(B) Late delay sample information aligned to whisker-rotor touch onset for cued recall versus control neurons.

(C) Sample information versus cross correlation of activity to whisker angle during the late delay for individual neurons.

(D) Sample information versus cross correlation of activity to whisker curvature change during the late delay for individual neurons.

(E) Cumulative probability distribution of response correlations to touch angle for neurons with cued recall versus control neurons.

(F) Cumulative probability distribution of response correlations to $\Delta\kappa$ for neurons with significant cued recall versus control neurons. n = 5,574 neurons. See also Figure S3.

the late delay period. These neurons showed increases in firing and sample information that were aligned to the onset of touch, demonstrating that this information followed whisker-rotor contact.

To investigate whether cued recall activity could reflect a sensorimotor cue that was present upon rotor re-approach, we examined whisker kinematics during the late delay period (Figure S3). No differences in curvature change ($|\Delta\kappa|$) were observed during this period ($p = 0.46$, paired t test). Depending on the sample stimulus, whisker angle differed by an average of 1.1° upon rotor re-contact ($p < 1 \times 10^{-6}$, paired t test). However, the magnitude of this whisker angle difference was below behaviorally reported thresholds of perceptual discrimination (Cheung et al., 2019). To test whether cued recall activity could be explained by tuning preferences to these whisker features, we compared each neuron's selectivity to touch angle and curvature change to the strength of cued recall response. Preference to touch angle was negatively correlated with cued responses, whereas curvature change was not correlated with cued recall response (angle: $R = -0.04$, $p < 0.002$; $|\Delta\kappa|$: $R = 0.004$, $p = 0.77$) (Figures 4C and 4D). Cued recall neurons encoded the whisker angle less reliably than other neurons, whereas no difference was found with respect to tuning for curvature change (Figures 4E and 4F) (angle: $p < 0.02$ and $|\Delta\kappa|$: $p = 0.78$, K-S test). Overall, these findings demonstrate that cued recall responses are not sufficiently explained by sensorimotor features alone, suggesting that they more likely reflect a retrieval of sample stimulus information from working memory.

Context-Dependent Responses during the Test Period

To understand how the recalled sample stimulus and incoming test stimulus are combined to generate categorical responses, we characterized neurons that exhibited context-modulated responses to either match or non-match conditions. For each context-modulated neuron, we determined the neuron's preferred tuning to stimulus direction (anterior or posterior) during the sample period and analyzed each trial condition with respect to the neuron's preferred direction (Figure 5A). We assessed how the firing rate to the preferred stimulus during the test period was modulated relative to the sample period (Figures 5B and S4). For match neurons, we observed a "match enhancement," in which the preferred stimulus response on match trials increased during the test period relative to the preferred stimulus response during the sample period (Figure 5C). On non-match trials, match neurons exhibited a "non-match suppression," in which the estimated firing rate for the preferred stimulus during the test period was lower than expected given the preferred stimulus response during the sample period. Whereas we identified one type of match neuron, we observed two types of non-match neurons. Type I non-match neurons expressed cued recall responses in the late delay period, whereas type II neurons did not. Type II non-match neurons were characterized by both non-match enhancement and match-suppression during the test period.

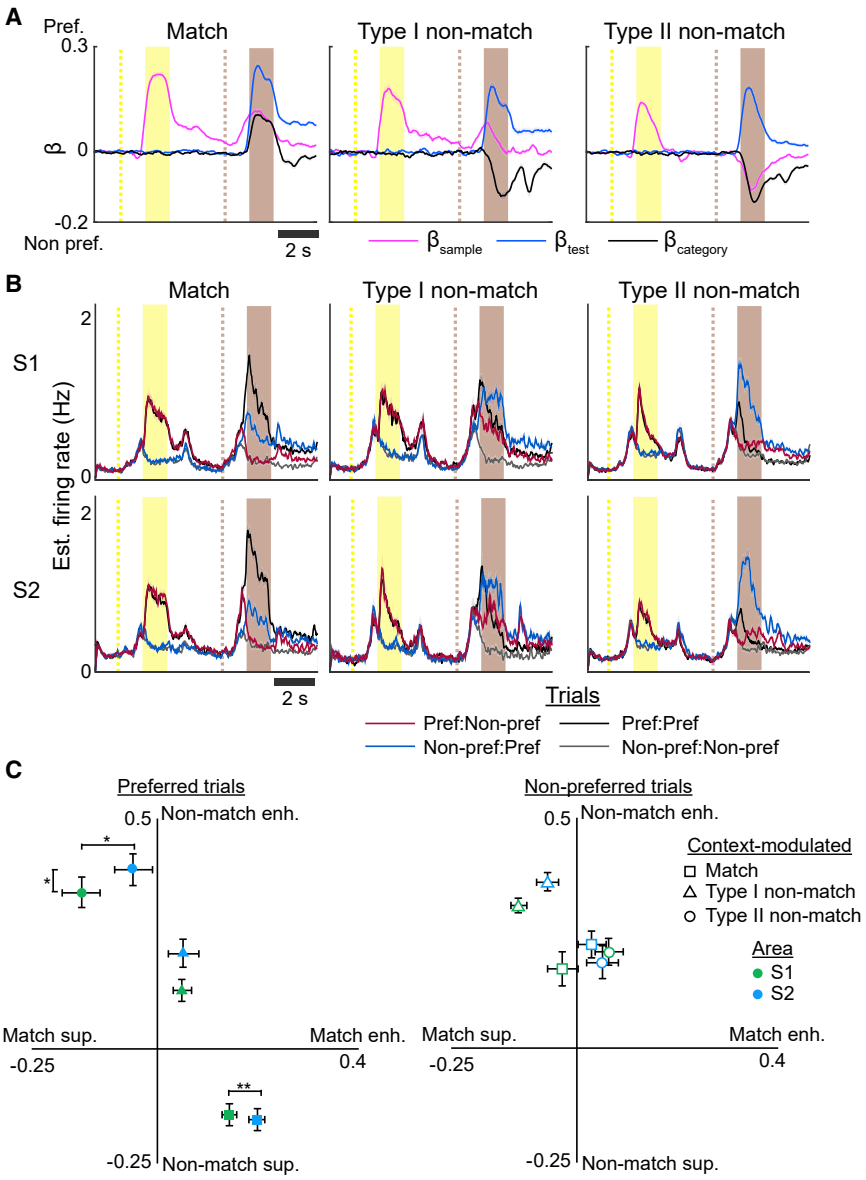

Figure 5. Match and Non-match Responses Reflect Context Modulation

(A) Encoding of β_{sample}, β_{test}, and $\beta_{category}$ across the trial period averaged across match and non-match neurons aligned to the preferred stimulus of each neuron.

(B) Estimated firing rate across match and non-match neurons in S1 and S2 for each trial condition aligned to the preferred stimulus of each neuron.

(C) Modulation in estimated firing rate during the test period relative to responses during the sample period with respect to the preferred (left) or non-preferred (right) stimulus direction. Error bars indicate SEM; n = 174 S1 match neurons, 155 S2 match neurons, 89 S1 type I non-match neurons, 65 S2 type II non-match neurons, 220 S1 type II non-match neurons, 148 S2 type II non-match neurons; *$p < 0.05$, **$p < 0.02$.

See also Figure S4.

Localized and Distributed Forms of Information Processing

Although stimulus, cued recall, and category information are heterogeneously represented across S1 and S2, such information could either reflect processing occurring locally in one area or processing that is distributed across areas. To resolve this, we tracked the flow of such information between areas along with area- and task-specific functional perturbations. To track information flow, responses in identified projection neurons between S1 and S2 were compared against unlabeled neurons in each of their respective areas (Figures 6A and S5A). To further delineate the role of each area during context-dependent sensory processing, we optogenetically inactivated each area by channelrhodopsin (ChR2)-mediated excitation of inhibitory neurons in task-performing VGAT-ChR2-EYFP mice (Zhao et al., 2011) (n = 6). Each area was silenced at four different time points during the trial: (1) in the sample period, (2) early in the delay period, (3) late in the delay period, and (4) in the test period (Figure 6B).

Type I non-match neurons differed from type II non-match neurons in that very little firing rate modulation was observed with respect to the neuron's preferred stimulus. Instead, these neurons exhibited non-match responses regardless of whether the preferred or non-preferred stimulus was presented during the sample period.

Overall, compared with S1 neurons, S2 neurons consistently exhibited stronger modulation. S2 match neurons showed greater match enhancement than S1 neurons ($p < 0.02$, independent t test). Compared with S1 neurons, type II non-match S2 neurons exhibited greater non-match enhancement but weaker match suppression (non-match enhancement: $p < 0.05$; non-match suppression: $p < 0.05$, independent t test). These results demonstrate a variety of forms of match and non-match signals, suggesting that different mechanisms could be involved in producing context-modulated responses.

Stimulus direction is already present in the ventral posterior medial (VPM) thalamus, which provides input to both S1 and S2 (Bale and Petersen, 2009; Narumi et al., 2007), suggesting that this information is processed by these areas in parallel. Indeed, inactivation of either S1 or S2 during the sample period did not affect task performance. Compared with $S1_{ND}$ and $S2_{ND}$ neurons, larger fractions of $S1_{S2}$ and $S2_{S1}$ neurons coding for stimulus direction were found ($S1_{S2}$ versus $S1_{ND}$: $p < 0.05$, $S2_{S1}$ versus $S2_{ND}$: $p < 0.02$; χ^2 test). This bidirectional flow of sensory information provides a form of compensation from inactivating one area versus the other. In contrast, inactivation of S2, but not S1, during the late delay period affected task

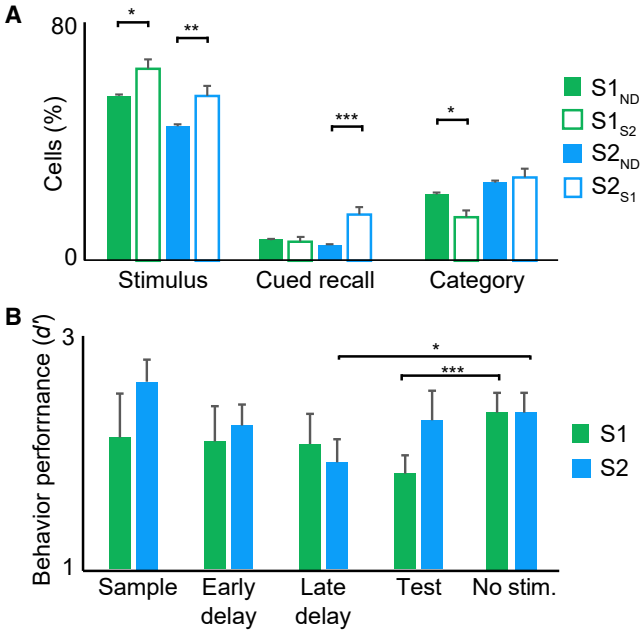

Figure 6. Distinct Requirement of Task Information in S1 and S2

(A) Fraction of neurons coding for stimulus, cued recall, and category information across anatomical cell types.

(B) Effect of optogenetic inactivation of S1 or S2 on behavioral performance. Error bars indicate SD from a bootstrap test (A), SEM (B); n = 6,603 neurons (A), n = 6 animals (B); *p < 0.05, **p < 0.02, ***p < 0.002.

See also Figure S5.

performance (late delay inactivation versus no inactivation: $p < 0.05$, paired t test), suggesting that S2 is important for processing cued recall responses. Such responses in S2 appeared to be relayed to S1, given that, compared with $S2_{ND}$ neurons, larger fractions of $S2_{S1}$ contained cued recall responses during the late delay period ($p < 1 \times 10^{-6}$, χ^2 test). Inactivation of S1, but not S2, during the test period affected task performance (test inactivation versus no inactivation: $p < 0.002$, paired t test). Although category information was found in both areas, $S1_{S2}$ neurons were underrepresented compared with $S1_{ND}$ neurons ($p < 0.05$, χ^2 test). This suggests that category responses in S1 and S2 are computed locally in each area but only responses in S1 are important for task performance through pathways that do not include S2. Inactivation of V1 did not produce any behavioral deficits, demonstrating that the functional effects observed in S1 and S2 were specific to those areas (Figure S5B). Overall, these results demonstrate that both localized and distributed processing schemes can combine to explain the heterogeneity of response properties across S1 and S2.

Cued Recall and Category Responses Are Modulated by Behavioral State

To further identify differences in task-related activity between S1 and S2, we investigated how such information in each area relates to task performance, first in regard to the animal's choice. Given that error trials were relatively infrequent (<15% of trials), we used linear discriminant analysis to model the population-level responses of stimulus, cued recall, and category by using correct trials (hit and correct rejection) and then tested the model's performance on error trials (miss or false alarm) (Figures 7A and S6). Encoding of stimulus information in either S1 or S2 did not depend on correct performance. However, encoding of cued recall information in both S1 and S2 decreased on miss trials but was not different during false alarm trials (S1: β_{sample} performance: correct, 69.9% ± 1.4%; error, 51.5% ± 3.3%; $p < 1 \times 10^{-4}$, paired t test; $\beta_{category}$ performance: correct, 73.2% ± 1.6%; error, 56.0% ± 2.0%; $p < 1 \times 10^{-9}$, paired t test; S2: β_{sample} performance: correct, 68.4% ± 1.7%; error, 50.4% ± 3.1%; $p < 1 \times 10^{-5}$, paired t test; $\beta_{category}$ performance: correct, 74.7% ± 1.5%; error, 65.5% ± 1.9%; $p < 1 \times 10^{-9}$, paired t test).

Decreased model performance on miss trials could reflect periods of disengagement as opposed to an incorrect choice. To resolve this, we tested whether cued recall and category information were present during the test period during conditions of passive stimulation. Overall, cued recall information was significantly reduced compared with during task performance but remained above chance levels (Figure 7B) (S1: task versus passive, $p < 1 \times 10^{-9}$; passive versus shuffle, $p < 1 \times 10^{-5}$; S2: task versus passive, $p = 0.0973$; passive versus shuffle, $p < 1 \times 10^{-6}$, paired t test). However, this information was less reduced in S2 compared with S1, suggesting that cued recall responses are more robustly maintained in S2 than S1 across behavioral states ($p < 0.002$, independent t test). Category responses were separated according to match ($+\beta_{category}$) and non-match ($-\beta_{category}$) conditions. Both were significantly reduced in S1 and S2 during passive conditions (S1: task versus passive, $p < 1 \times 10^{-9}$; passive versus shuffle, $p < 1 \times 10^{-3}$; S2: task versus passive, $p < 1 \times 10^{-9}$; passive versus shuffle, $p < 1 \times 10^{-5}$, paired t test) (Figures 7C and 7D). However, match responses were less reduced in S2 compared with S1 ($p < 0.05$, independent t test). Non-match responses in S2 remained significantly above chance, but not in S1 (S1: task versus passive, $p < 1 \times 10^{-9}$; passive versus shuffle, $p = 0.08$; S2: task versus passive, $p < 1 \times 10^{-9}$; passive versus shuffle, $p < 0.05$, paired t test). Overall, these results demonstrate that cued recall and category responses can be behaviorally modulated in S1 and S2. However, such information is more reliably present in S2 when animals are not engaged in the task.

S1 and S2 Differ in Their Network Properties

The stronger context modulation and greater persistence of cued recall and category responses during passive conditions in S2 suggest that network properties might differ between S1 and S2. We analyzed the trial-by-trial shared response variability between neuronal pairs (also known as "noise correlations"), which has been linked to neurobiological mechanisms that include activation by common input, recurrent local interactions, inter-areal communication, and state-dependent modulation (Cohen and Kohn, 2011). We compared neuronal pairs with significant stimulus, cued recall, or category responses within S1, within S2, and between S1 and S2. We found no difference in correlated variability between pairs within S1 for all three response types during the test period (Figure 8A). However, in S2, neuronal pairs encoding cued recall or category

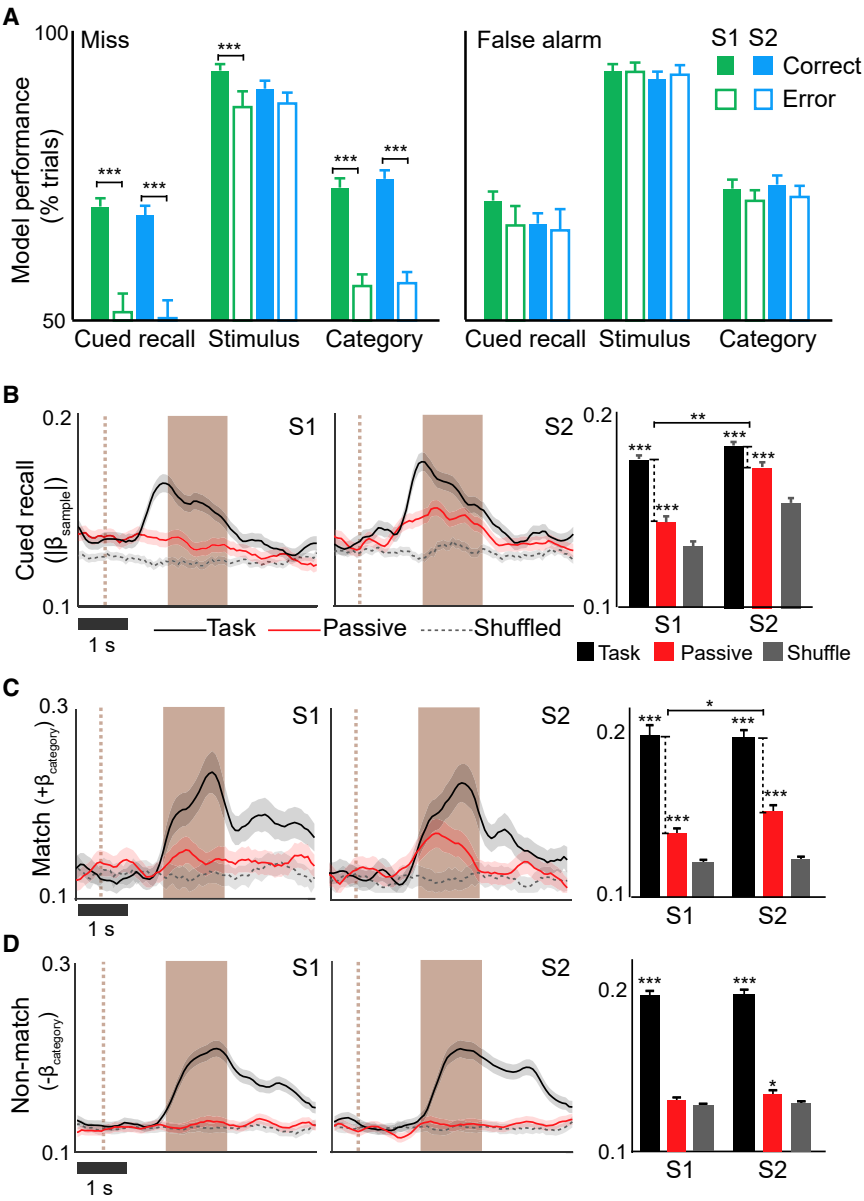

Figure 7. Cued Recall and Category Responses Are Differentially Task Modulated across S1 and S2

(A) Population coding of stimulus, cued recall, or category information during the test period analyzed according to the animal's choice by using cross-validation. Performance of a classifier modeled from correct trials are shown upon testing on other correct trials (solid bars) or error trials (open bars). Testing was performed separately for S1 or S2 on either miss trials (left) or false alarm trials (right).

(B–D) Comparison of sample recall and category information during the test period under task performance versus passive stimulation in S1- and S2-cued recall encoding neurons (B), match encoding neurons (C), and non-match encoding neurons (E) are shown. Left indicates the average time course during the test period for active, passive, and shuffled conditions. Right indicates mean across the test period. Error bars indicate SEM; n = 57 imaged populations (A), 583 S1 neurons, 473 S2 neurons (B), 95 S1 neurons, 102 S2 neurons (C), 454 S1 neurons, and 421 S2 neurons (D); *p < 0.05, **p < 0.02, ***p < 1×10^{-3}.

See also Figure S6.

responses exhibited stronger correlated variability than those encoding stimulus responses (cued recall versus stimulus: $p < 0.05$; category versus stimulus: $p < 0.05$, paired t test). These differences were also observed when analyzing activity during the sample period, suggesting that this correlated variability reflects a network property of S2 that spans the trial period (Figure 8B) (cued recall versus stimulus: $p < 0.05$; category versus stimulus: $p < 0.05$, paired t test). No differences were observed between neuronal pairs between S1 and S2, suggesting that correlation patterns in S2 do not reflect global fluctuations. This finding indicates that correlated variability among cued recall and category neurons in S2 reflect local functional subnetworks.

Because correlated variability can influence population coding (Averbeck et al., 2006), we examined how S1 and S2 neurons participated in encoding cued recall and category responses at the population level. Using linear discriminant analysis, we assessed the population-level responses of cued recall and category information while varying the fraction of simultaneously imaged neurons included in analysis. We observed that population representations of cued recall and category information in S2 are less reliably encoded with fewer neurons than S1 (Figures 8C and 8D). Together, this suggests that cued recall and category responses in S2 rely on local population interactions from functionally similar neurons. This reinforcement of responses might facilitate the encoding of such information in individual neurons across behavioral states.

DISCUSSION

In conclusion, our study resolves how local processing and interareal interactions between S1 and S2 can produce distributed activity patterns encoding stimulus, cued recall, and category responses. We identify both similarities and differences in how each area produces these responses and how they are relevant to task performance. During the sample period, S1 and S2 are individually dispensable for task performance, suggesting that stimulus direction is inherited from VPM (Bale and Petersen, 2009; Narumi et al., 2007) and processed in parallel in both areas. Bi-directional cortico-cortical flow of stimulus information

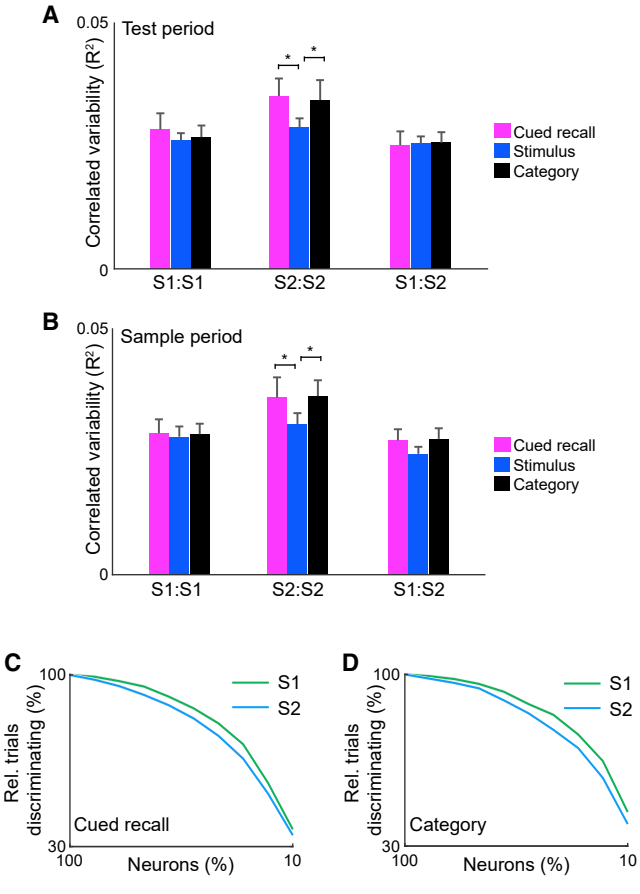

Figure 8. Network Differences between S1 and S2

(A) Mean correlated variability during the test period from simultaneously imaged neurons of similar response properties for neuronal pairs within S1 (S1:S1), within S2 (S2:S2), and between S1 and S2 (S1:S2).

(B) Mean correlated variability during the sample period from simultaneously imaged neurons of similar response properties for neuronal pairs within S1 (S1:S1), within S2 (S2:S2), and between S1 and S2 (S1:S2).

(C) Population discriminability of cued recall information in S1 versus S2 as function of fraction of simultaneously imaged neurons included for linear discriminant analysis.

(D) Population discriminability of category information in S1 versus S2 as function of fraction of simultaneously imaged neurons included for linear discriminant analysis.

n = 57 imaged populations. *p < 0.05. Error bars indicate SEM.

might further provide compensation to maintain overall function when either area is inactivated during this period (Minamisawa et al., 2018). Experiments involving pathway-specific perturbation or where S1 and S2 are dually inactivated might help to support this idea.

Although persistent working memory activity was not observed in S1 or S2, we have identified a cued recall response in these areas. Although such a response has been observed in S2 of non-human primates (Romo and de Lafuente, 2013), this is the first report of this information in S1. We find that cued recall is specifically processed in S2 and relayed to S1. How this cued recall responses arises in S2 is unclear, and the underlying mechanisms warrant future investigation. We speculate that areas encoding the working memory that are connected to S2 might alter the gain of tactile responses to facilitate the recalled response upon whisker touch, similar to what has been described in the visual system (Merrikhi et al., 2017). Evidence suggests that this might be further enabled by network properties specific to S2. This is reflected in stronger functional coupling among cued recall neurons, which could allow such information to more readily persist across task and passive conditions. This functional coupling could be explained by higher degrees of recurrent connectivity enabling integration of information across longer timescales (Goldin et al., 2018; Runyan et al., 2017), specific long-range input from areas related to mnemonic processing (Ährlund-Richter et al., 2019; Kealy and Commins, 2011), or potential differences in cellular properties that enables the maintenance of information at a synaptic level (Mongillo et al., 2008).

The availability of cued recall and incoming stimulus information in both S1 and S2 suggest that each area is able to locally generate context-modulated responses in the form of match and non-match signals. Local circuit mechanisms through inhibitory interactions between match and non-match neurons have been proposed to explain such responses but warrant future investigation (Engel and Wang, 2011; Machens et al., 2005). Whereas match and non-match responses are stronger in S2, those signals in S1 appear specifically relevant for task performance. This suggests a distinction in how each area is handling this information. Given that S2 is not the major output of the categorical information that exists in S1, it suggests that S1 might play a role in relaying this information to other areas, such as the primary motor cortex or striatum (Chen et al., 2013; Lee et al., 2019). If this is the case, the effect of S1 inactivation during the test period reflects the importance of S1 pathways that directly connect sensory processing to decision making and motor execution, which will require further investigation.

In contrast, we propose that categorical responses in S2 might primarily be relevant for the learning and recollection of such stimulus associations that are secondarily used for decision making. This explains the behavioral effect of S2 inactivation during the late delay, but not the test, period. Recent studies investigating S1 and S2 during tactile detection or discrimination tasks have demonstrated that choice-related activity emerges through learning (Chen et al., 2015; Yamashita and Petersen, 2016) from an inter-areal loop in which choice-related activity in S1 is inherited from S2 (Chen et al., 2016; Kwon et al., 2016; Ni and Chen, 2017; Yang et al., 2016). We propose that choice activity described in prior tasks reflects a stimulus-outcome association rather than the decision signal driving behavior. Although disambiguating the two phenomena by using previous task designs is not possible, our task reveals the importance of S2 in retrieving prior stimulus information, which reflects the general ability for S2 to assign context to stimulus information whether the context is a behavioral outcome or prior sensory information. Given its connectivity as a hub in between S1 and the perirhinal cortex, S2 is well situated to mediate the acquisition and reinforcement of such contextual associations. Investigating S2's interactions with perirhinal cortex and during task learning will help to

further resolve its role in processing stimulus context and in behavior. Overall, our results bridge a local circuit and long-range network understanding for the role of S1 and S2 during context-dependent sensory processing, expanding our view for how these areas participate in perception and behavior.

STAR★METHODS

Detailed methods are provided in the online version of this paper and include the following:

- KEY RESOURCES TABLE
- LEAD CONTACT AND MATERIALS AVAILABILITY
- EXPERIMENTAL MODEL AND SUBJECT DETAILS
  - Mice
- METHOD DETAILS
  - Animal preparation
  - Cortical mapping
  - Behavioral task
  - Optogenetic inactivation
  - Multi-area two-photon imaging
- QUANTIFICATION AND STATISTICAL ANALYSIS
  - Calcium imaging processing
  - Whisker tracking and analysis
  - Multiple regression analysis
  - Choice-related stimulus information
  - Cued recall and category information during passive stimulation
  - Context modulation
  - Network analysis
- DATA AND CODE AVAILABILITY

SUPPLEMENTAL INFORMATION

Supplemental Information can be found online at https://doi.org/10.1016/j.neuron.2020.02.004.

ACKNOWLEDGMENTS

We thank M. Valley and N. Li for guidance in optogenetic inactivation experiments and C. Harvey, M. Howe, S. Kira, and B. Scott for comments on the manuscript. This work was supported by grants from a NARSAD Young Investigator Grant from the Brain & Behavior Research Foundation, the Richard and Susan Smith Family Foundation, Elizabeth and Stuart Pratt Career Development Award, the Whitehall Foundation, National Science Foundation Neuronex Neurotechnology Hub (NEMONIC #1707287), National Institutes of Health BRAIN Initiative Award (R01NS109965), National Institutes of Health New Innovator Award (DP2NS111134), National Institutes of Health Ruth L. Kirschstein Predoctoral Individual National Research Service Award (F31NS111896) to C.C., and Boston University Center for Systems Neuroscience Post-Doctoral Fellowship to J.N. and E.L.

AUTHOR CONTRIBUTIONS

J.L.C. designed the study. C.C., J.N., and J.L.C. performed two-photon imaging experiments. E.L., J.N., N.J., and J.L.C. performed data analysis. K.B., T.O., and E.L. performed optogenetics experiments. C.C., E.L., and J.L.C. wrote the paper.

DECLARATION OF INTERESTS

The authors declare no competing interests.

Received: May 13, 2019
Revised: November 11, 2019
Accepted: February 6, 2020
Published: March 11, 2020

REFERENCES

Ährlund-Richter, S., Xuan, Y., van Lunteren, J.A., Kim, H., Ortiz, C., Pollak Dorocic, I., Meletis, K., and Carlén, M. (2019). A whole-brain atlas of monosynaptic input targeting four different cell types in the medial prefrontal cortex of the mouse. Nat. Neurosci. *22*, 657–668.

Averbeck, B.B., Latham, P.E., and Pouget, A. (2006). Neural correlations, population coding and computation. Nat. Rev. Neurosci. *7*, 358–366.

Bale, M.R., and Petersen, R.S. (2009). Transformation in the neural code for whisker deflection direction along the lemniscal pathway. J. Neurophysiol. *102*, 2771–2780.

Bethge, P., Carta, S., Lorenzo, D.A., Egolf, L., Goniotaki, D., Madisen, L., Voigt, F.F., Chen, J.L., Schneider, B., Ohkura, M., et al. (2017). An R-CaMP1.07 reporter mouse for cell-type-specific expression of a sensitive red fluorescent calcium indicator. PLoS ONE *12*, e0179460.

Chen, J.L., Carta, S., Soldado-Magraner, J., Schneider, B.L., and Helmchen, F. (2013). Behaviour-dependent recruitment of long-range projection neurons in somatosensory cortex. Nature *499*, 336–340.

Chen, J.L., Margolis, D.J., Stankov, A., Sumanovski, L.T., Schneider, B.L., and Helmchen, F. (2015). Pathway-specific reorganization of projection neurons in somatosensory cortex during learning. Nat. Neurosci. *18*, 1101–1108.

Chen, J.L., Voigt, F.F., Javadzadeh, M., Krueppel, R., and Helmchen, F. (2016). Long-range population dynamics of anatomically defined neocortical networks. eLife *5*, e14679.

Cheung, J., Maire, P., Kim, J., Sy, J., and Hires, S.A. (2019). The sensorimotor basis of whisker-guided anteroposterior object localization in head-fixed mice. Curr Biol. *29*, 3029–3040.e4.

Clack, N.G., O'Connor, D.H., Huber, D., Petreanu, L., Hires, A., Peron, S., Svoboda, K., and Myers, E.W. (2012). Automated tracking of whiskers in videos of head fixed rodents. PLoS Comput. Biol. *8*, e1002591.

Cohen, M.R., and Kohn, A. (2011). Measuring and interpreting neuronal correlations. Nat. Neurosci. *14*, 811–819.

DiCarlo, J.J., Zoccolan, D., and Rust, N.C. (2012). How does the brain solve visual object recognition? Neuron *73*, 415–434.

Engel, T.A., and Wang, X.J. (2011). Same or different? A neural circuit mechanism of similarity-based pattern match decision making. J. Neurosci. *31*, 6982–6996.

Felleman, D.J., and Van Essen, D.C. (1991). Distributed hierarchical processing in the primate cerebral cortex. Cereb. Cortex *1*, 1–47.

Fisher, R. (1936). The use of multiple measurements in taxonomic problems. Ann. Eugen. *7*, 179–188.

Friedrich, J., Zhou, P., and Paninski, L. (2017). Fast online deconvolution of calcium imaging data. PLoS Comput. Biol. *13*, e1005423.

Goldin, M.A., Harrell, E.R., Estebanez, L., and Shulz, D.E. (2018). Rich spatiotemporal stimulus dynamics unveil sensory specialization in cortical area S2. Nat. Commun. *9*, 4053.

Hernández, A., Nácher, V., Luna, R., Zainos, A., Lemus, L., Alvarez, M., Vázquez, Y., Camarillo, L., and Romo, R. (2010). Decoding a perceptual decision process across cortex. Neuron *66*, 300–314.

Jun, J.J., Steinmetz, N.A., Siegle, J.H., Denman, D.J., Bauza, M., Barbarits, B., Lee, A.K., Anastassiou, C.A., Andrei, A., Aydın, Ç., et al. (2017). Fully integrated silicon probes for high-density recording of neural activity. Nature *551*, 232–236.

Kealy, J., and Commins, S. (2011). The rat perirhinal cortex: A review of anatomy, physiology, plasticity, and function. Prog. Neurobiol. *93*, 522–548.

Khan, A.G., and Hofer, S.B. (2018). Contextual signals in visual cortex. Curr. Opin. Neurobiol. *52*, 131–138.

Kitada, R. (2016). The Brain Network for Haptic Object Recogniton. In Pervasive Haptics: Science, Design, and Application, H. Kajimoto, S. Saga, and M. Konyo, eds. (Springer Japan), pp. 21–37.

Koay, S.A., Thiberge, S.Y., Brody, C.D., and Tank, D.W. (2019). Neural correlates of cognition in primary visual versus neighboring posterior cortices during visual evidence-accumulation-based navigation. bioRxiv, 568766.

Kwon, S.E., Yang, H., Minamisawa, G., and O'Connor, D.H. (2016). Sensory and decision-related activity propagate in a cortical feedback loop during touch perception. Nat. Neurosci. *19*, 1243–1249.

Lee, C.R., Yonk, A.J., Wiskerke, J., Paradiso, K.G., Tepper, J.M., and Margolis, D.J. (2019). Opposing influence of sensory and motor cortical input on striatal circuitry and choice behavior. Curr. Biol. *29*, 1313–1323.e5.

Machens, C.K., Romo, R., and Brody, C.D. (2005). Flexible control of mutual inhibition: a neural model of two-interval discrimination. Science *307*, 1121–1124.

Margolis, D.J., Lütcke, H., Schulz, K., Haiss, F., Weber, B., Kügler, S., Hasan, M.T., and Helmchen, F. (2012). Reorganization of cortical population activity imaged throughout long-term sensory deprivation. Nat. Neurosci. *15*, 1539–1546.

Merrikhi, Y., Clark, K., Albarran, E., Parsa, M., Zirnsak, M., Moore, T., and Noudoost, B. (2017). Spatial working memory alters the efficacy of input to visual cortex. Nat. Commun. *8*, 15041.

Miller, E.K., Li, L., and Desimone, R. (1991). A neural mechanism for working and recognition memory in inferior temporal cortex. Science *254*, 1377–1379.

Minamisawa, G., Kwon, S.E., Chevee, M., Brown, S.P., and O'Connor, D.H. (2018). A non-canonical feedback circuit for rapid interactions between somatosensory cortices. Cell Rep. *23*, 2718–2731.e6.

Minderer, M., Brown, K.D., and Harvey, C.D. (2019). The spatial structure of neural encoding in mouse posterior cortex during navigation. Neuron *102*, 232–248.e11.

Mongillo, G., Barak, O., and Tsodyks, M. (2008). Synaptic theory of working memory. Science *319*, 1543–1546.

Narumi, T., Nakamura, S., Takashima, I., Kakei, S., Tsutsui, K., and Iijima, T. (2007). Impairment of the discrimination of the direction of single-whisker stimulation induced by the lemniscal pathway lesion. Neurosci. Res. *57*, 579–586.

Ni, J., and Chen, J.L. (2017). Long-range cortical dynamics: a perspective from the mouse sensorimotor whisker system. Eur. J. Neurosci. *46*, 2315–2324.

O'Connor, D.H., Clack, N.G., Huber, D., Komiyama, T., Myers, E.W., and Svoboda, K. (2010). Vibrissa-based object localization in head-fixed mice. J. Neurosci. *30*, 1947–1967.

Ohkura, M., Sasaki, T., Kobayashi, C., Ikegaya, Y., and Nakai, J. (2012). An improved genetically encoded red fluorescent Ca2+ indicator for detecting optically evoked action potentials. PLoS ONE *7*, e39933.

Pnevmatikakis, E.A., and Giovannucci, A. (2017). NoRMCorre: An online algorithm for piecewise rigid motion correction of calcium imaging data. J. Neurosci. Methods *291*, 83–94.

Pnevmatikakis, E.A., Soudry, D., Gao, Y., Machado, T.A., Merel, J., Pfau, D., Reardon, T., Mu, Y., Lacefield, C., Yang, W., et al. (2016). Simultaneous denoising, deconvolution, and demixing of calcium imaging data. Neuron *89*, 285–299.

Romo, R., and de Lafuente, V. (2013). Conversion of sensory signals into perceptual decisions. Prog. Neurobiol. *103*, 41–75.

Romo, R., Lemus, L., and de Lafuente, V. (2012). Sense, memory, and decision-making in the somatosensory cortical network. Curr. Opin. Neurobiol. *22*, 914–919.

Rumelhart, D.E., and McClelland, J.L. (1987). Parallel distributed processing: explorations in the microstructure of cognition. Foundations *1*, 1–567.

Runyan, C.A., Piasini, E., Panzeri, S., and Harvey, C.D. (2017). Distinct timescales of population coding across cortex. Nature *548*, 92–96.

Saunders, A., Johnson, C.A., and Sabatini, B.L. (2012). Novel recombinant adeno-associated viruses for Cre activated and inactivated transgene expression in neurons. Front. Neural Circuits *6*, 47.

Siegel, M., Buschman, T.J., and Miller, E.K. (2015). Cortical information flow during flexible sensorimotor decisions. Science *348*, 1352–1355.

Sofroniew, N.J., Flickinger, D., King, J., and Svoboda, K. (2016). A large field of view two-photon mesoscope with subcellular resolution for in vivo imaging. eLife *5*, e14472.

Steinmetz, N., Zatka-Haas, P., Carandini, M., and Harris, K. (2018). Distributed correlates of visually-guided behavior across the mouse brain. bioRxiv, 474437.

Tervo, D.G., Hwang, B.Y., Viswanathan, S., Gaj, T., Lavzin, M., Ritola, K.D., Lindo, S., Michael, S., Kuleshova, E., Ojala, D., et al. (2016). A designer AAV variant permits efficient retrograde access to projection neurons. Neuron *92*, 372–382.

Xue, M., Atallah, B.V., and Scanziani, M. (2014). Equalizing excitation-inhibition ratios across visual cortical neurons. Nature *511*, 596–600.

Yamashita, T., and Petersen, C.Ch. (2016). Target-specific membrane potential dynamics of neocortical projection neurons during goal-directed behavior. eLife *5*, 5.

Yang, H., Kwon, S.E., Severson, K.S., and O'Connor, D.H. (2016). Origins of choice-related activity in mouse somatosensory cortex. Nat. Neurosci. *19*, 127–134.

Zhao, S., Ting, J.T., Atallah, H.E., Qiu, L., Tan, J., Gloss, B., Augustine, G.J., Deisseroth, K., Luo, M., Graybiel, A.M., and Feng, G. (2011). Cell type–specific channelrhodopsin-2 transgenic mice for optogenetic dissection of neural circuitry function. Nat. Methods *8*, 745–752.

STAR★METHODS

KEY RESOURCES TABLE

REAGENT or RESOURCE	SOURCE	IDENTIFIER
Bacterial and Virus Strains		
AAV-PHP.eb-syn-RCaMP1.07	Bethge et al., 2017	N/A
retroAAV-syn-Flpo	Xue et al., 2014	Addgene Cat #60663
AAV2.1-Ef1α-dio-eGFP	Saunders et al., 2012	Addgene Cat #37084
retroAAV-syn-Cre	James M. Wilson	Addgene Cat #10553
AAV2.1-Ef1α-fio-mCardinalNLS	This paper	N/A
AAV2.1-Ef1α-fio-mTagBFP2H2B	This paper	N/A
Experimental Models: Organisms/Strains		
C57BL/6J mice	The Jackson Laboratory	JAX:000664
VGAT-ChR2-EYFP mice	The Jackson Laboratory	JAX:014548
Software and Algorithms		
Motion Correction	Pnevmatikakis and Giovannucci, 2017	https://github.com/flatironinstitute/NoRMCorre
Calcium Source Extraction	Pnevmatikakis et al., 2016	https://github.com/flatironinstitute/CaImAn-MATLAB
Calcium Deconvolution	Friedrich et al., 2017	https://github.com/j-friedrich/OASIS
Whisker Tracking	Clack et al., 2012	https://www.janelia.org/open-science/whisk-whisker-tracking
MATLAB	Mathworks	https://www.mathworks.com/products/matlab.html
LabVIEW	National Instruments	https://www.ni.com/en-us/shop/labview.html

LEAD CONTACT AND MATERIALS AVAILABILITY

Further information and requests for resources and reagents should be directed to and will be fulfilled by the Lead Contact, Jerry Chen (jerry@chen-lab.org). All unique/stable reagents generated in this study are available from the Lead Contact with a completed Materials Transfer Agreement.

EXPERIMENTAL MODEL AND SUBJECT DETAILS

Mice

All experimental procedures were approved by the Institutional Animal Care and Use Committee for the Charles River Campus at Boston University. Imaging experiments were performed on young adult (6-8 weeks old) male C57BL/6J mice (The Jackson Laboratory). Optogenetic inactivation experiments were performed on young adult (6-8 weeks old) male VGAT-ChR2-EYFP mice (The Jackson Laboratory). Mice were housed 1–2 per cage in reverse 12 h light cycle conditions. All handling and behavior occurred under simulated night time conditions. No statistical methods were used to predetermine sample size. Since animals constituted one experimental group, experiments were not randomized and the investigators were not blinded to allocation during experiments and outcome assessment.

METHOD DETAILS

Animal preparation

For imaging experiments, stereotaxic viral injections were performed in S1 and S2 to express the genetically encoded calcium indicator, RCaMP1.07 in both areas and to label $S1_{S2}$ and $S2_{S1}$ neurons. One solution was prepared containing AAV-PHP.eb-syn-RCaMP1.07, retroAAV-syn-Flpo, and AAV2.1-Ef1α-dio-eGFP (600 nL total volume, ~1×10^9 vg/mL per virus, 2:1:1 ratio by volume) was delivered into one cortical area. Another solution was prepared containing AAV-PHP.eb-syn-RCaMP1.07, retroAAV-syn-Cre, and either AAV2.1-Ef1α-fio-mCardinalNLS or AAV2.1-Ef1α-fio-mTagBFP2H2B (600 nL total volume, ~1×10^9 vg/mL per virus, 2:1:1 ratio by volume) was delivered into another cortical area. To control for potential variability in viral titer that might selectively labeling $S1_{S2}$ or $S2_{S1}$ neurons, the two solutions were alternately delivered between areas from animal to animal. L2/3 and L5 of S1 was targeted at 1.1mm posterior to bregma, 3.3mm lateral, 300 and 500 μm below the pial surface. L2/3 and L5 of S2 was targeted at 0.7mm posterior to bregma, 4.2 lateral, 300 and 500 μm below the pial surface. For both imaging and optical inactivation

experiments, optical access over S1 and S2 was achieved by cranial window implantation (Margolis et al., 2012). A metal headpost for head fixation was implanted on the skull surrounding the window. One week after window implantation, animals were handled and head-fixed for increasing amounts of time up to 15 min to acclimate them for behavior experiments.

Cortical mapping

In order to select specific whisker regions for imaging and optogenetic inactivation, functional mapping was performed using optical intrinsic signal imaging (ISI) for S1 and a combination of ISI and two-photon calcium imaging for S2. For ISI, the animal was anesthetized with 1.5% isoflurane. The cortical surface was illuminated with a 625-nm LED (Thor Labs). Individual whiskers were stimulated at 10 Hz with a piezo-electric stimulator. Reflectance images were collected through a f = 25mm lens (Navitar) using a CMOS Camera (Hamamatsu; 6.5 um pixel size, 4 × 4 binning, 512 × 512 binned pixels, 30 Hz frame rate). Changes in reflectance during stimulation compared to pre-stimulation were expressed as $\Delta R/R$ (150 frame average). Barrel columns were identified as signal minima after averaging intrinsic reflectance signals over 10 trials. A blood vessel map of the cortical area surface was obtained with a 470 nm LED (Thor Labs) for registration and targeting of regions. In situations where ISI maps in S2 were weak, regions were identified and selected for by two-photon calcium imaging of RCamp1.07 signals following whisker stimulation. Whiskers were trimmed to a single row corresponding to the selected imaging or stimulation region.

Behavioral task

The whisker-based delayed non-match to sample task was performed using a custom written LabVIEW software (National Instruments) to control hardware and a data acquisition interface (USB-6008; National Instruments) for measuring licks, water delivery, and air puff delivery. A water port was attached to a capacitive lick sensor (AT42QT1010; SparkFun) that dispenses 5 to 6 uL of water through a miniature solenoid valve (0127; Buekert). For the rotation stimulus, commercial grade sandpaper (3M; roughness: P100) was mounted along the outside edge of a 6 cm diameter rotor, attached to a stepper motor (Zaber) to deflect the whiskers which was mounted onto a linear stage (Zaber) to place the rotor within whisker reach. Go and no-go trials were presented randomly at 50% probability each, with a maximum of three consecutive presentations of the same trial type. For the final task, the trial structure consisted of the following: 2 s baseline period, 1.2 s sample stimulus rotation, 2 s delay, 1.2 s test stimulus rotation, 2 s report period, and 1 s inter-trial period. The rotor was moved into position prior to the sample and test period and out of position following the sample and report period with 0.6 s travel time for each movement. Licking during go trials (non-match; sample $\neq$ test) was regarded as a "hit" trial and the animal received a water reward upon licking. No lick on a go trial was regarded as a "miss." No lick on no go trials was regarded a "correct reject," which was unrewarded. Licking on a no go trial (match; sample = test) was considered a "false alarm" during which no reward was given. Typically, each false alarm was punished with an air puff and ~7 s timeout before the next trial, but the strength of punishment varied for individual animals depending on its effects on behavioral performance. A metric of animal performance (d') was calculated for each session and defined as $d' = Z(\text{Hit}/(\text{Hit} + \text{Miss})) - Z(\text{FA})/(\text{FA} + \text{CR}))$, Where Hit is the number of hits, Miss is the number of misses, CR is the number of correct rejects, and FA is the number of false alarms. $Z(p) \in [0, 1]$ is the inverse of the cumulative Gaussian distribution for $p = Z(\text{Hit}/(\text{Hit} + \text{Miss}))$ or $Z(\text{FA})/(\text{FA} + \text{CR}))$.

Animals were water-deprived throughout the experiment. Task training proceeded through four stages. The goal of the first stage was to train the animal to reliably trigger the lick sensor to retrieve water. The second stage involved training animals to the task procedure. In this version of the go no-go task, one of the two go trials conditions and both no-go trial conditions were used. There was no delay period between sample and test period and the rotor remained in contact with the whisker throughout the sample and test period. During the third stage, the remaining go trial condition was introduced and the animals were trained to respond appropriately to all for four possible combinations of stimulus conditions. During the fourth stage, the delay was introduced beginning at 100ms with gradual increasing intervals until 2 s was reached. During this portion of training when the delay period was increased, the rotor remained in contact with whisker throughout the delay period. Once animals could reliably perform the task with a 2 s delay, the rotor was then moved out of position during the delay period. For stages 2-4, animals proceeded to the next stage of training once performance reached $d' > 1.75$ (80% correct performance) for two consecutive sessions. Behavior sessions were performed twice per day. Imaging or optogenetic inactivation experiments began once animals in the fourth session reached $d' > 1.75$ (80% correct performance) for two consecutive sessions completed were imaged *in vivo* during behavior when. Imaging during passive stimulation conditions occurred immediately following the end of behavioral session.

Optogenetic inactivation

Experiments were performed with a modified ISI system which enabled a 473 nm laser with built-in digital and analog modulation (Omnicron) to be coupled to a 2D scanning galvo system (Thorlabs), and then focused onto the brain surface through a f = 25mm lens (Navitar). Photo-stimulation consisted of a sinusoidal temporal profile (40 Hz) with a time average power of 2-8mW across ~1 mm^2. Since whiskers were trimmed to a single row, the area of inactivation may not completely overlap with all spared S1 barrel columns. To prevent the mice from distinguishing photostimulation trials from control trials using visual cue, a "masking flash" (40, 1 ms pulses at 10 Hz) was delivered using a blue LED near the eyes and sustained throughout the behavior session. For some sessions, only one cortical area was randomly stimulated at a frequency of 25% of trials. For other sessions in which stimulation randomly alternated between S1 and S2, each area was stimulated at a frequency of 15% of trials. For each stimulated

trial, the time window of stimulation was randomly selected between the sample, early delay, late delay, and test period. For each animal, > 100 photo-stimulation trials were performed per area and per trial period across multiple sessions. Animal performance (*d'*) was calculated for each photo-stimulation condition and compared to no stimulation using paired t test. The Bonferroni-Holm method was used to correct for multiple comparisons.

Multi-area two-photon imaging

Imaging was performed with a custom-built resonant-scanning multi-area two-photon microscope controlled by custom-written Scope software based on a design previously described (Chen et al., 2016). *In vivo* calcium imaging of RCaMP1.07 imaging was performed using a 40 Mhz 1040 nm fiber laser (Spark Lasers) split into two temporally multiplexed beams positioned over S1 and S2 through a 16x/0.8NA water immersion objective (Nikon) and simultaneously imaged at 32.6 Hz frame rate $S1_{S2}$ and $S2_{S1}$ projection neurons were identified *in vivo* either during the behavioral session using 1040 nm excitation when mCardinal or eGFP were expressed and resolved using 697/75 nm 525/45 nm filters (AVR Optics), respectively. When mTagBFP2 was expressed, labeled cells were identified at the end of the behavior session by 860 nm excitation with a Ti:sapphire laser (Mai Tai HP; Spectra Physics) and resolved with a 458/64 nm filter (AVR Optics).

QUANTIFICATION AND STATISTICAL ANALYSIS

Calcium imaging processing

All image processing was performed in MATLAB (Mathworks). Two-photon images were first processed for motion correction using a piece-wise rigid motion correction algorithm (Pnevmatikakis and Giovannucci, 2017). Regions of interest corresponding individual active neuron were identified and calcium signals by constrained non-negative matrix factorization (Pnevmatikakis et al., 2016). Deconvolution of calcium signals was performed to obtain a measure of estimated spike rate for individual neurons across the imaging period (Friedrich et al., 2017).

Whisker tracking and analysis

The whisker field was illuminated with 940-nm infrared LED light and movies were acquired at 500 Hz using a high-speed CMOS camera at 31.6 pixel/mm resolution (CL600x2; Optronis). For analysis, whiskers were automatically traced as described previously (Clack et al., 2012). Four out of 57 imaging sessions were excluded from analysis due to sub-optimal imaging conditions. The angle, curvature, and location of the whisker tip at each time point was extracted for all traced whiskers. The position of the rotor was automatically tracked in the video using custom scripts (MATLAB). Whisker-rotor touch was scored as events in which the tip of at least one whisker came into within < 5 pixel radius of the rotor face. Whisker kinematics during the pre-sample period and the late delay period were compared by taking the mean angle or curvature across a 600ms window prior to rotor movement before sample stimulus delivery (pre-sample) or test stimulus delivery (late delay).

For cross-correlation analysis of kinematic parameters to deconvolved calcium signals, time vectors of kinematic parameters were downsampled to the imaging frame rate and analysis was carried out on the first 600 ms (~20 frames) after whisk-rotor touch during the late delay period. Trial-by-trial cross correlation was performed for neuronal activity against curvature change ($|\Delta\kappa|$), which was calculated as the absolute difference between the mean curvature for 600ms prior to and following whisk-rotor touch during the late delay period. For whisker angle, the mean whisker angle following whisker-rotor touch was separated into binary vectors representing a range of angles from -90° to 90°, subdivided at 2° intervals. Each sub-vector reflects the likelihood that the whisker angle falls within that given angle range. Cross correlation was performed on each sub-vector and the overall correlation to whisker angle was obtained by taking the maximum R value across the sub-vectors.

Multiple regression analysis

To assess neuronal response to task stimuli, we performed a multiple regression analysis to model the deconvolved calcium signals as follows:

$$Y(t) = \beta_0(t) + \beta_{\text{sample}}(t)x_{\text{sample}} + \beta_{\text{test}}(t)x_{\text{test}} + \beta_{\text{category}}(t)x_{\text{category}} \quad (1)$$

where $Y(t)$ is the estimated firing rate at time t, β_0 is the baseline regressor, β_{sample} is the regressor for the sample stimulus x_{sample} ('anterior' or 'posterior'), β_{test} is the regressor for the test stimulus x_{test} ('anterior' or 'posterior'), and β_{category} is the regressor for the trial category $x_{category}$ ('match' or 'non-match'). In cases in which the time course of regressors across the trial period was analyzed, deconvolved calcium signals were first smoothed (±150ms), down-sampled (60ms bins) and z-scored before applying the multiple regression. In cases in which regressors were analyzed with respect to discrete time windows during the trial period, deconvolved calcium signals were down-sampled to each time window and z-transformed before applying the multiple regression. To assess the significance of each regressor, a shuffled population distribution was obtained by deriving coefficients from data with shuffled trial-condition labels for each neuron, repeated 1000 times. A statistical threshold was applied to identify significant coefficient values as defined as $p < 0.001$ above shuffled conditions.

Choice-related stimulus information

Cross-validation was used to assess the encoding of cued recall, stimulus, and category information in S1 or S2 as a function of the animal's choice. Since error trials (miss or false alarm) constituted < 15% of tasks trials, information encoding was assessed at a population level as opposed to across individual neurons. We used linear discriminant analysis (LDA) for dimensionality reduction of neuronal population responses. Observations consisted of the average estimated firing rate across a 600ms period prior to the onset of the test stimulus (for cued recall activity) or following the onset of the test stimulus (for stimulus- and category-related activity) for all neurons simultaneously recorded within an imaging field, thus representing the neuronal state space vector at this moment (with each neuron representing one dimension) as 'snapshot' of the state space vector trajectory during the given trial.

Observations were divided into test data or training data. Test data included either all n error trials or an equal number of randomly selected correct trials (hit and correct rejection) from an imaging session. Training data included all remaining correct trials not selected as training data. A classifier was trained using LDA in which trials were separated into the N_1 and N_2 trials for the two chosen trial conditions C_1 and C_2, respectively (e.g., anterior versus posterior deflection during the test period for cued recall, anterior versus posterior deflection during the test period and stimulus information; match versus non-match for category information). Estimated single-neuron firing rate were arranged in a matrix $\mathbf{x}$ with neurons as columns and trials as rows. The LDA procedure seeks to find a projection vector w such that the projections of the observations onto this axis, collected in the vector:

$$y = w^T \mathbf{x} + w_0 \tag{2}$$

are best separated for the two chosen trial conditions. Maximal separation is defined as the maximal difference of the mean vectors $\mu_1 = (1/N_1)\sum_{n\in C_1} x_n$ and $\mu_2 = (1/N_2)\sum_{n\in C_2} x_n$ for C_1 and C_2, respectively, normalized by the within-class scatter. The solution, known as Fisher's linear discriminant (Fisher, 1936), is given by

$$w^T = S_w^{-1}(\mu_1 - \mu_2) \tag{3}$$

where S_W^{-1} is the within-class covariance given by

$$S_W^{-1} = \sum_{n\in C_1}(x_n - \mu_1)(x_n - \mu_1)^T + \sum_{n\in C_2}(x_n - \mu_2)(x_n - \mu)^T \tag{4}$$

The bias is calculated as

$$w_0 = -\frac{1}{2}\left(w^T\mu_1 - w^T\mu_2\right) \tag{5}$$

Intuitively, this procedure finds a hyperplane in the state space (orthonormal to the projection vector w and encompassing w_0) providing best separation given the Fisher's criterion. For cross-validation, activity data from the remaining test trials were projected onto the same hyperplane as the classifier. Receiver operating characteristic (ROC) analysis was used to assess how well the classifier predicted trial conditions C_1 and C_2 in the test data. This process was repeated 1000 times and the average was taken as the performance for each imaging plane. Classifier performance between correct and error trials was compared using independent t test. The Bonferroni-Holm method was used to correct for multiple comparisons.

Cued recall and category information during passive stimulation

To compare encoding of cued recall and category information between task and passive stimulation conditions, we subsampled the task trials (~300 trials) to match the fewer passive trials (~50trials, sessions with less than 10 passive trials were excluded) for each session. Passive trials were collected after the mouse stopped performing the task. Since relatively few passive trials (~50) were collected for each neuron compared to task trials (~300), task trials were subsampled. Multiple regression analysis was performed after randomly selected a number of active trials equal to the number of passive trials for each neuron. In addition, a population null distribution was obtained by performing multiple regression analysis on shuffled condition labels for each neuron. Differences in regressors between task versus passive conditions was compared using paired t test. The significance of regressors during passive conditions was determined by comparing passive conditions to regressors from shuffled conditions and assessed using paired t test. Differences in strength of task modulation between S1 and S2 were assessed using independent t test. The Bonferroni-Holm method was used to correct for multiple comparisons.

Context modulation

A modulation index (MI) was calculated to assess how firing rates differed between the sample and test period as a function of a neuron's tuning. The preferred tuning of a neuron with respect to anterior or posterior deflection of the whisker was determined by computing the average β_{test} across a 600ms period following test stimulus onset where $\beta_{test} > 0$ reflected a neuron tuned to anterior deflections and $\beta_{test} < 0$ reflected a neuron tuned to posterior deflections. Modulation index against the neuron's preferred direction with respect to match trials was calculated as $MI_{match} = (F_{match} - F_{\underline{sample}})/(F_{match} + F_{sample})$ where F_{sample} was the average firing rate over the 600 ms period following sample onset from trials in which the preferred stimulus was presented and where F_{match} was the average firing rate over the 600 ms period following test onset from match trials in which the preferred stimulus

was presented. $MI_{match} > 0$ was considered 'match enhancement' whereas $MI_{match} < 0$ was considered 'match suppression'. Modulation index against the neuron's preferred direction with respect to match trials was calculated as $MI_{non\text{-}match} = (F_{non\text{-}match} - F_{sample})/(F_{non\text{-}match} + F_{sample})$ where F_{sample} was the average firing rate over the 600 ms period following sample onset from trials in which the preferred stimulus was presented and where F_{match} was the average firing rate over the 600 ms period following test onset from non-match trials in which the preferred stimulus was presented. $MI_{non\text{-}match} > 0$ was considered 'non-match enhancement' whereas $MI_{non\text{-}match} < 0$ was considered 'non-match suppression'. Similar modulation indexes against the non-preferred direction were also calculated with respect to match and non-match trials. Modulation indexes across different match and non-match neurons in S1 and S2 were compared using independent t test.

Network analysis

Trial-by-trial correlated variability in neuronal activity (R^2) was calculated for each pair of neurons. For the sample period, the mean estimated firing rate over a 1 s period following sample onset was used. For the test period, the mean estimated firing rate over a 1 s period following test onset was used. For each neuronal pair, correlated variability was separately calculated for each of the four trial conditions. Neuronal pairs were grouped based on similar response properties according to whether they share significant β_{sample}, β_{test}, or $\beta_{category}$ of the same sign (ie. pairs of category neurons would either be both $+\beta_{category}$ or both $-\beta_{category}$). A population level measure of correlated variability was obtained by taking the mean R^2 across all trial conditions for all simultaneously imaged pairs within a recording session. Correlated variability of between neuronal pairs of different response properties were compared using paired t test. The Bonferroni-Holm method was used to correct for multiple comparisons.

To assess the robustness of populating coding across varying neuronal population sizes, LDA followed by (ROC) analysis was used to assess the population-level discriminability. Observations consisted of the average estimated firing rate across a 600ms period prior to the onset of the test stimulus (for cued recall activity) or following the onset of the test stimulus (for category activity). For each imaging session, population size was varied by randomly excluding fractions of neurons at 10% intervals and computing the discriminability for the remaining neuron in the population. This process was repeated 1000 times and the average discriminability was used to reflect the discriminability at a given population size. Relative discriminability was determined by normalizing discriminability to that determined from including all possible simultaneously imaged neurons.

DATA AND CODE AVAILABILITY

Data and code used in this study are available upon request.